Supporting Online Material

Structure of the Nociceptin/Orphanin FQ Receptor in Complex with a Peptide Mimetic

Aaron A. Thompson[1§], Wei Liu[1§], Eugene Chun[1§], Vsevolod Katritch[1], Huixian Wu[1], Eyal Vardy[2], Xi-Ping Huang[2], Claudio Trapella[3], Remo Guerrini[3], Girolamo Calo[4], Bryan L. Roth[2], Vadim Cherezov[1], Raymond C. Stevens[1*]

[1]Department of Molecular Biology, The Scripps Research Institute, La Jolla, CA 92037, USA

[2]National Institute of Mental Health Psychoactive Drug Screening Program, Department of Pharmacology and Division of Chemical Biology and Medicinal Chemistry, University of North Carolina Chapel Hill Medical School, Chapel Hill, NC 27599, USA

[3]Department of Pharmaceutical Sciences and LTTA (Laboratorio per le Tecnologie delle Terapie Avanzate), University of Ferrara, 44121 Ferrara, Italy

[4]Department of Experimental and Clinical Medicine, Section of Pharmacology and National Institute of Neuroscience, University of Ferrara, 44121 Ferrara, Italy

[§]These authors contributed equally to this work

[*]Address correspondence to: The Scripps Research Institute, 10550 North Torrey Pines Rd., GAC-1200, La Jolla, CA 92037. Tel.: 858-784-9416; Fax: 858-784-9483; E-mail: stevens@scripps.edu.

Supplementary Tables:

Supplementary Table 1. Summary of crystallographic and structure refinement data

Structure	BRIL-NOP receptor	
Data collection		
Number of crystals	23	
Space group	*P2$_1$*	
Cell dimensions a, b, c (Å)	42.1, 170.9, 65.4	
β (degrees)	103.1	
Number of reflections measured	48,462	
Number of unique reflections	16,545	
Resolution (Å)	50 – 3.0 (3.11 – 3.0)[1]	
R_{merge} (%)	19.4 (66.0)	
$\langle I \rangle / \langle \sigma(I) \rangle$	8.5 (2.0)	
Completeness (%)	93.3 (79.5)	
Multiplicity	2.9 (2.1)	
Refinement		
Resolution (Å)	32 – 3.0	
R-work (%)	24.8	
R-free (%)	28.9	
Number of atoms	A	B
Receptor	2113	2081
BRIL	N/A	813
Ligand	32	32
Lipids/Water	41	18
Overall B value (Å^2)	A	B
Receptor	70.4	65.6
BRIL	N/A	90.7
Ligand	64.7	60.3
Lipids/Water	74.3	56.0
R.m.s. deviations		
Bond lengths (Å)	0.003	
Bond angles (°)	0.56	
Ramanchandran plot statistics (%)*		
Favored regions	97.04	
Allowed regions	2.96	
Disallowed regions	0.0	

[1]Data in parentheses are for the highest resolution shell.
[2]As defined in MolProbity[1]

Supplementary Table 2. Comparative ligand binding profile of NOP receptor expressed in HEK 293-T cells and engineered NOP constructs expressed in *Sf9* insect cells.

Compound	WT-NOP expressed in HEK293-T cells	FL-NOP expressed in *Sf9* cells	NOP-ΔC expressed in *Sf9* cells	BRIL-ΔN-NOP-ΔC expressed in *Sf9* cells
N/OFQ	0.3, (9.5 ± 0.07)	0.6, (9.22 ± 0.05)	1.3, (8.9 ± 0.09)	0.6, (9.2 ± 0.07)
SCH-221510	2.5, (8.6 ± 0.1)	25, (7.6 ± 0.12)*	25, (7.6 ± 0.14)*	32, (7.5 ± 0.1)*
C-24	0.3, (9.5 ± 0.08)	0.5 (9.3 ± 0.06)	2.0, (8.7 ± 0.08)	3.2, (8.5 ± 0.08)
C-35	0.3, (9.5 ± 0.07)	0.5, (9.3 ± 0.07)	3.2, (8.5 ± 0.1)	5.0, (8.3 ± 0.07)*

Data represent K_i (nM), (pK_i ± sem) for competition binding experiments using ^{3}H-N/OFQ (0.2-0.3 nM final concentration). All *Sf9* expressed constructs, including the full-length (FL) version contain a FLAG tag and 10His tag at the N- and C- terminus, respectively, whereas the WT-NOP construct is devoid of tags. The K_i for SCH-221510 (agonist) is attenuated upon expression in *Sf9* cells. Compound-24 (C-24) and Compound-35 (C-35) are slightly attenuated by C-terminal truncation of the receptor. *$p < 0.05$.

Supplementary Table 3. NOP agonist-mediated $G_{i/o}$ activation in HEK 293-T cells.

Construct	EC_{50}(nM), (pEC_{50} ± sem)	
	N/OFQ	SCH-221510
WT NOP	1.7, (8.76 ± 0.04)	6.6, (8.18 ± 0.06)
NOP-ΔC	18, (7.75 ± 0.07)	107, (6.97 ± 0.11)
BRIL-ΔN-NOP	29, (7.54 ± 0.06)	83, (7.08 ± 0.05)
BRIL-ΔN-NOP-ΔC[1]	87, (7.06 ± 0.22)	1905, (5.72 ± 0.30)

[1]Construct BRIL-ΔN-NOP-ΔC had maximal cAMP inhibition of 50% relative to the wild type construct (NOP receptor).

Measurement of cAMP response as an indicator of $G_{i/o}$ activation in HEK293-T cells using a cAMP biosensor (for details see Kimple et al., 2009[2]). The data represent EC_{50} (nM), (pEC_{50} ± sem) from three experiments in quadruplicate. The different construct were cloned into pCDNA3.1 and expressed in HEK 293-T cells: NOP receptor (wild type), NOP-ΔC, BRIL-ΔN-NOP, and BRIL-ΔN-NOP-ΔC were all sequence optimized for expression in *Sf9* cells. Agonist response was attenuated by the protein engineering, as can be seen by the decreased potency in NOP-ΔC and BRIL-ΔN-NOP, and decreased potency and efficacy in BRIL-ΔN-NOP-ΔC.

Supplementary Table 4. Effect of NOP mutations on agonist induced $G_{i/o}$ activation.

Construct	EC_{50} (nM), (pEC_{50} ± sem)	
	N/OFQ	SCH-221510
WT NOP	1.6, (8.79 ± 0.14)	15, (7.83 ± 0.16)
Q107A	531, (6.28 ± 0.12)	1622, (5.79 ± 0.18)
D110A	1172, (5.86 ± 0.06)	31, (7.50 ± 0.16)
D130A	1012, (6.00 ± 0.06)	2770, (5.56 ± 0.12)
Y131A	206, (6.69 ± 0.11)	318, (6.50 ± 0.2)
M134A	8.3, (8.08 ± 0.18)	20, (7.69 ± 0.29)
I219A	30, (7.52 ± 0.29)	251, (6.60 ± 0.30)
Q280A	234, (6.62 ± 0.27)	944, (6.03 ± 0.44)
Y309A	11, (7.96 ± 0.36)	1412, (5.85 ± 0.20)

Measurement of cAMP response as an indicator of $G_{i/o}$ activation; the data represent EC_{50} (nM), (pEC_{50} ± sem) from a minimum of three experiments conducted in quadruplicate in transfected HEK 239-T cells. The D110A mutation affected N/OFQ potency the most, but did not affect that of SCH-221510. The M134A mutation had the least effect on both N/OFQ and SCH-221510 potency. All mutants significantly affected agonist potency ($p<0.05$).

Supplementary Table 5. Effect of NOP mutations on antagonist inhibition of agonist (N/OFQ) induced $G_{i/o}$ activation.

Construct	K_i (nM), (pK_i ± sem)	
	Compound-24	**Compound-35**
WT NOP	3.2, (8.50 ±0.19)	11, (7.95 ± 0.22)
Q107A	32, (7.49 ± 0.10)*	71, (7.15 ± 0.11)*
D110A	3.8, (8.42 ± 0.06)	20, (7.71 ± 0.13)
D110A (SCH-221510)[1]	3.5, (8.46 ± 0.18)	19, (7.71 ± 0.05)
D130A	>10,000	>10,000
Y131A	19, (7.73 ± 0.17)*	68, (7.17 ± 0.14)*
M134A	0.5, (9.28 ± 0.24)	2.1, (8.67 ± 0.22)
I219A	0.3, (9.52 ± 0.57)	3.3, (8.48 ± 0.35)
Q280A	28, (7.55 ± 0.14)*	83, (7.08 ± 0.03)*
Y309A	>10,000	>10,000

[1]D110A mutant was also tested with SCH-221510 as agonist, since SCH-221510 was not affected by the mutation.

Measurement of cAMP response as an indicator of $G_{i/o}$ activation; the data represent K_i values (nM), (pK_i or ± sem) from a minimum of three experiments conducted in quadruplicate. K_i values were estimated from the functional assay using Cheng-Prusoff equation ($K_i = IC_{50}/(1+L/EC_{50})$, in which EC_{50} is agonist (N/OFQ or SCH-221510) potency determined from an agonist concentration-response curve; L is agonist (N/OFQ or SCH-221510) concentration used in the antagonist assay; IC_{50} is the concentration of testing drug at which N/OFQ or SCH-221510-mediated $G_{i/o}$ activation was inhibited by 50% in HEK 293-T cells. *$p < 0.05$ vs. WT.

Supplementary Figures:

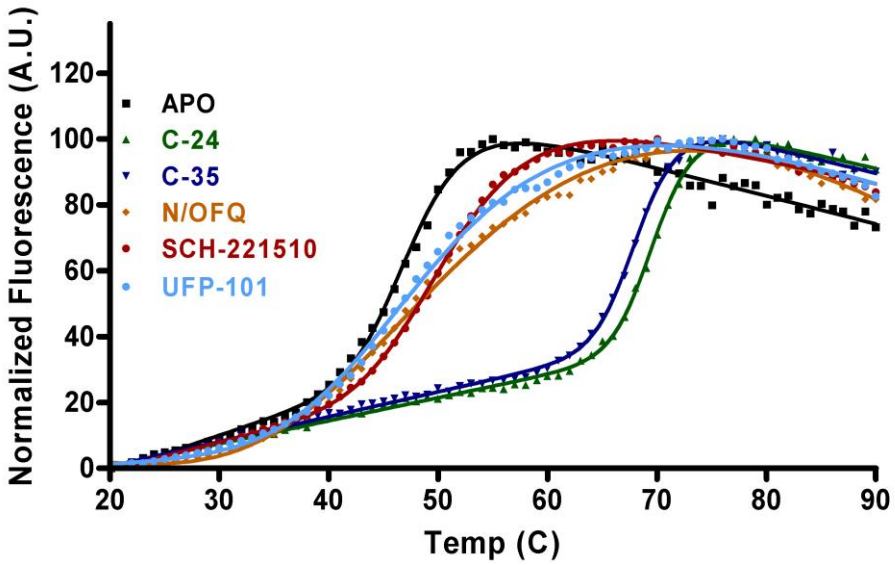

Supplementary Figure 1. Thermal stability conferred on the BRIL-ΔN-NOP-ΔC receptor construct by agonists and antagonists. Thermal stability data collected by thermal ramping in the presence of a thiol-reactive N-[4-(7-diethylamino-4-methyl-3-coumarinyl)phenyl]maleimide (CPM) fluorophore [3,4]. The thermostability of the NOP receptor increased from 48.0 ± 0.2 °C (Apo) to 52.0 ± 0.2 °C in the presence of SCH-221510, 53 ± 1 °C in the presence of UFP-101, 56 ± 4 °C in the presence of N/OFQ, 68.4 ± 0.1 °C in the presence of C-35, and 70.0 ± 0.1 °C in the presence of C-24. All compounds were tested at a concentration of 5 μM. Midpoints of the thermal transitions were obtained using a least squares non-linear regression analysis (GraphPad Prism) as described in Thompson et al., 2010[4].

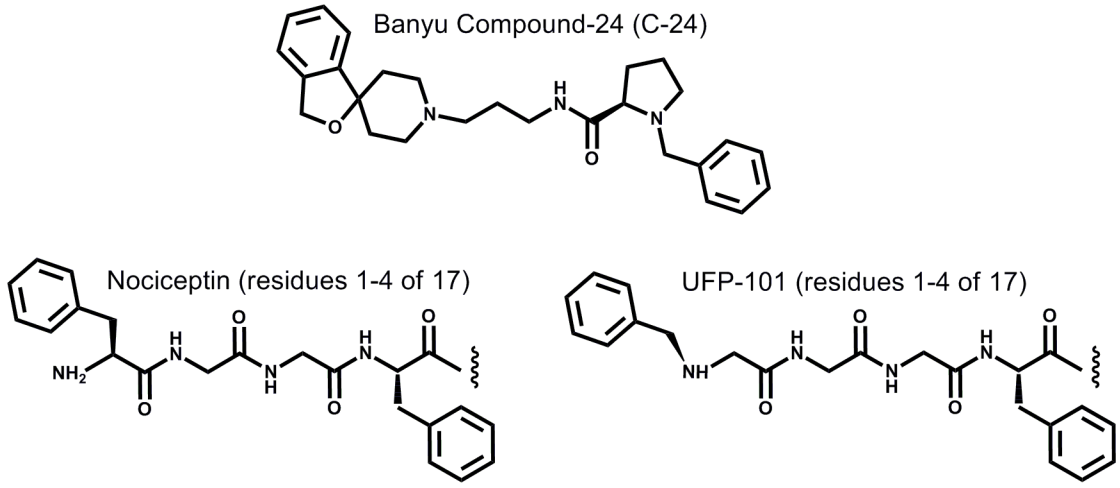

Supplementary Figure 2. Chemical structure comparison of C-24, and the N-terminal four amino acid residues of N/OFQ (agonist) and UFP-101 (antagonist).

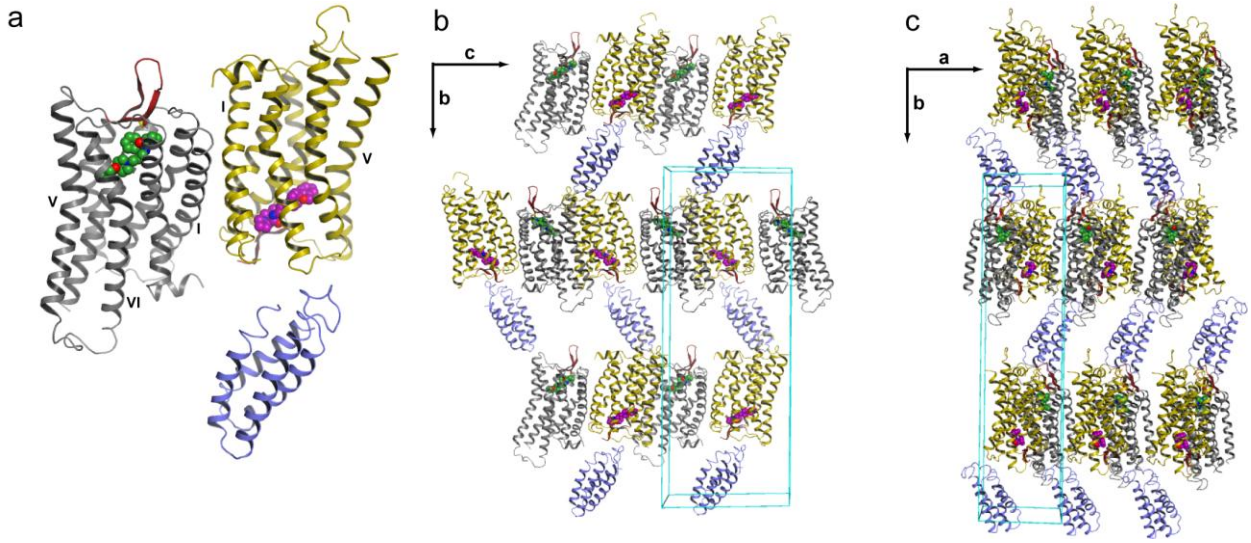

Supplementary Figure 3. The asymmetric unit and crystal lattice packing of BRIL-ΔN-NOP-ΔC. (**a**) The asymmetric unit of the BRIL-ΔN-NOP-ΔC (abbreviated as BRIL-NOP in the manuscript) construct consisting of two antiparallel NOP receptor molecules colored gray (molecule A) and yellow (molecule B), and one BRIL domain colored blue, which forms crystal lattice contacts with two receptors from an adjacent layer. (**b**) (**c**) Two different views of the $P2_1$ lattice highlighting the layered type I crystal packing that has been observed in all membrane protein crystals grown in LCP.

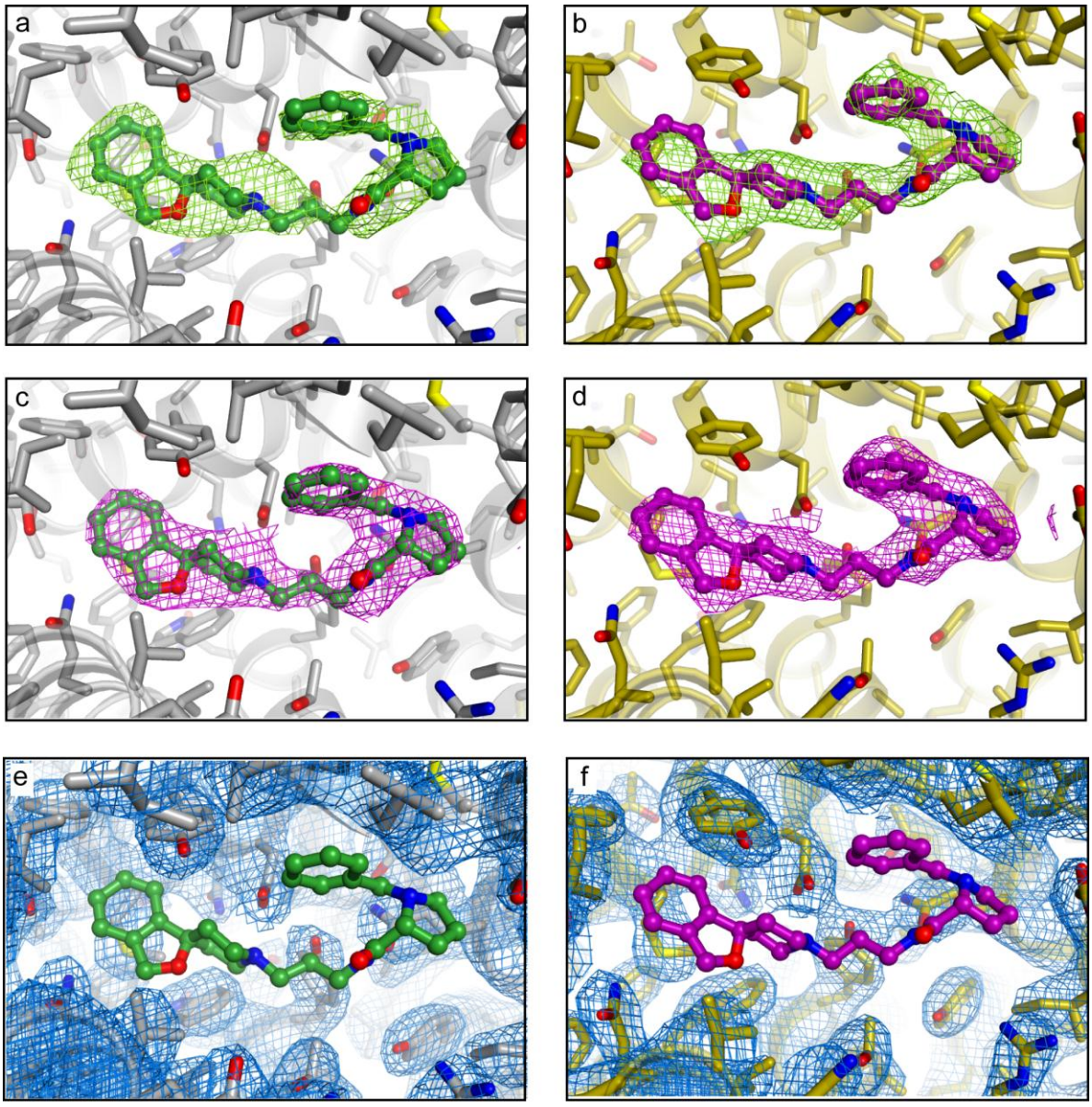

Supplementary Figure 4. **Examples of the electron density maps calculated from the refined model for the BRIL-NOP/C-24 complex**. $|F_o|-|F_c|$ omit maps (green mesh) of the ligand C-24 in (**a**) the 'A' receptor and (**b**) 'B' receptor within one asymmetric unit, contoured at 2.5 σ (0.0203 e/Å^3). The $|F_o|-|F_c|$ omit map was calculated after removal of the ligand and 25 interations of coordinate/B-factor refinement. $2|F_o|-|F_c|$ maps (magenta mesh) contoured at 1.0 σ (0.0173 e/Å^3) around C-24 in (**c**) receptor 'A' and (**d**) receptor 'B'. $2|F_o|-|F_c|$ maps (blue mesh) contoured at 1.0 σ. (0.0173 e/Å^3) around protein residues of the orthosteric pocket in (**e**) receptor 'A' and (**f**) receptor 'B'. All maps were generated with a carve radius of 1.75 Å.

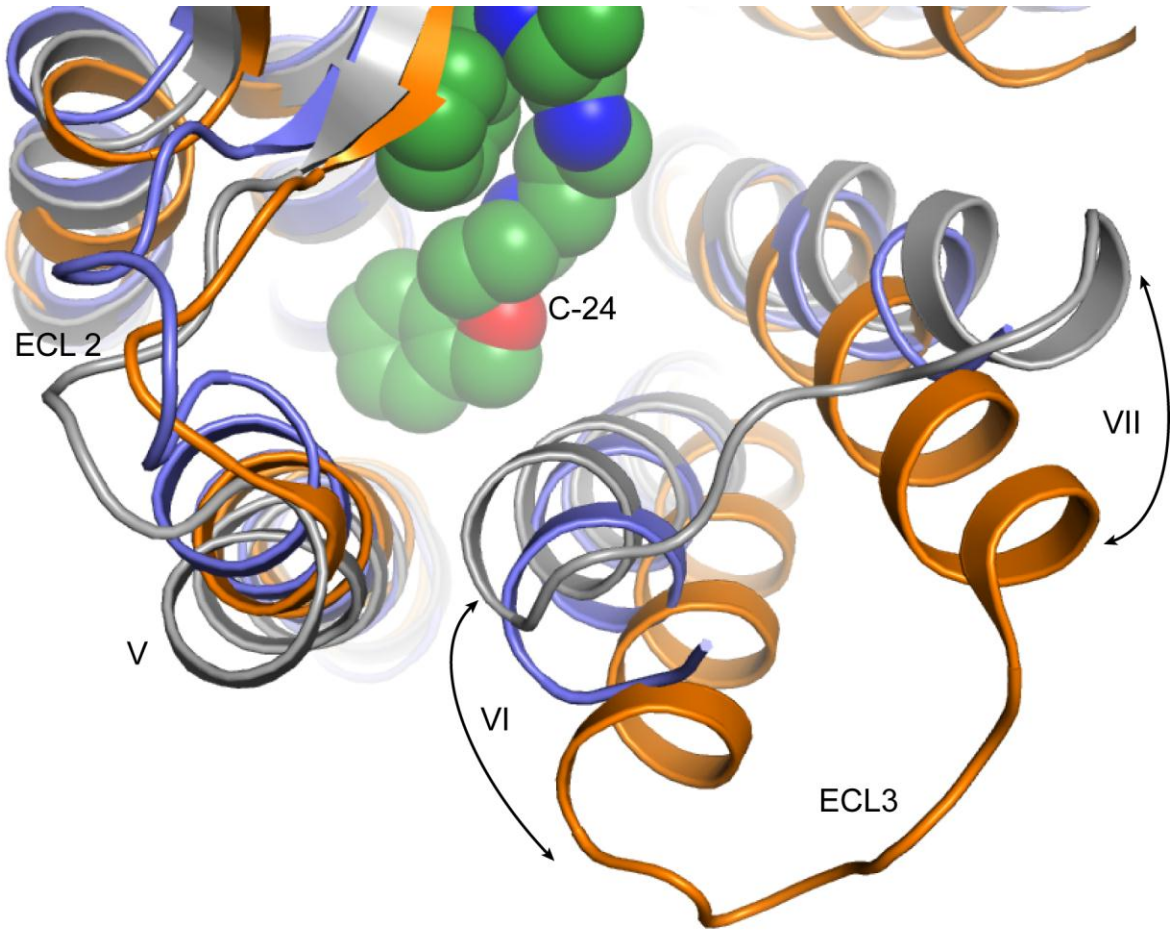

Supplementary Figure 5. Conformational differences between the EC region of NOP, κ-OR and CXCR4. Structural alignment of NOP (gray with C-24 depicted as green spheres), κ-OR[5] (PDB ID 4DJH; blue), and CXCR4[6] (PDB ID 3ODU; orange) showing conformational differences centered around the extracellular regions of helices V, VI and VII.

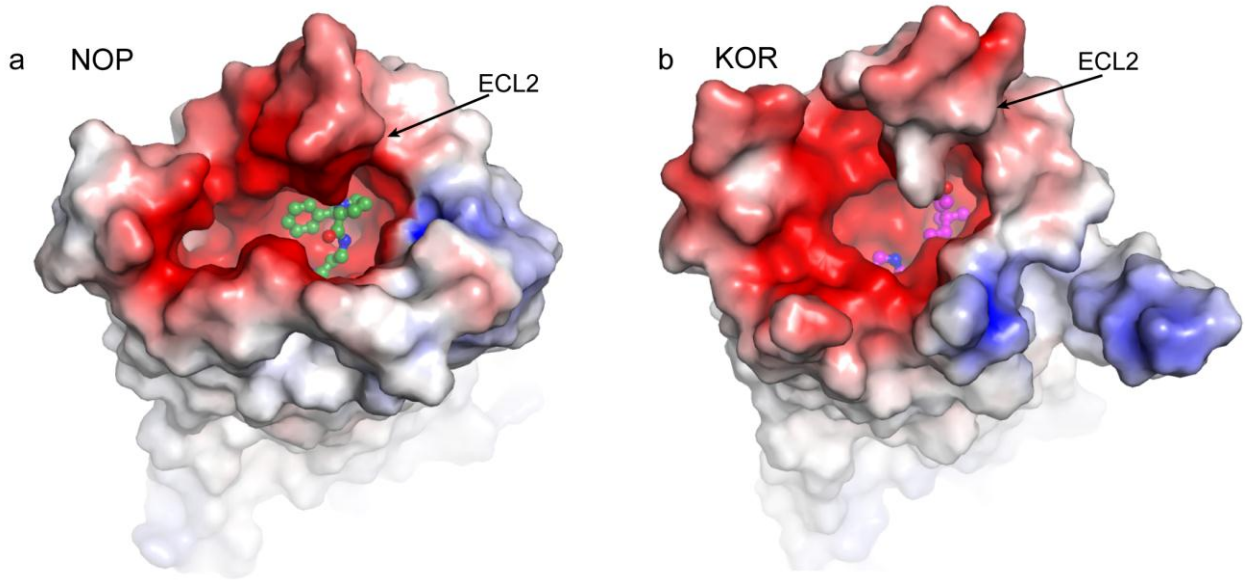

Supplementary Figure 6. Comparison of the electrostatic potential surface of NOP versus κ-OR. Electrostatic surface potentials of (**a**) NOP and (**b**) κ-OR (PDB ID 4DJH) colored blue to red, corresponding to positive and negative surface potentials (+5 to -5 kT/e), respectively. Differences in the electrostatics and topology at the entrance of the orthosteric binding pocket likely play a role in peptide selectivity.

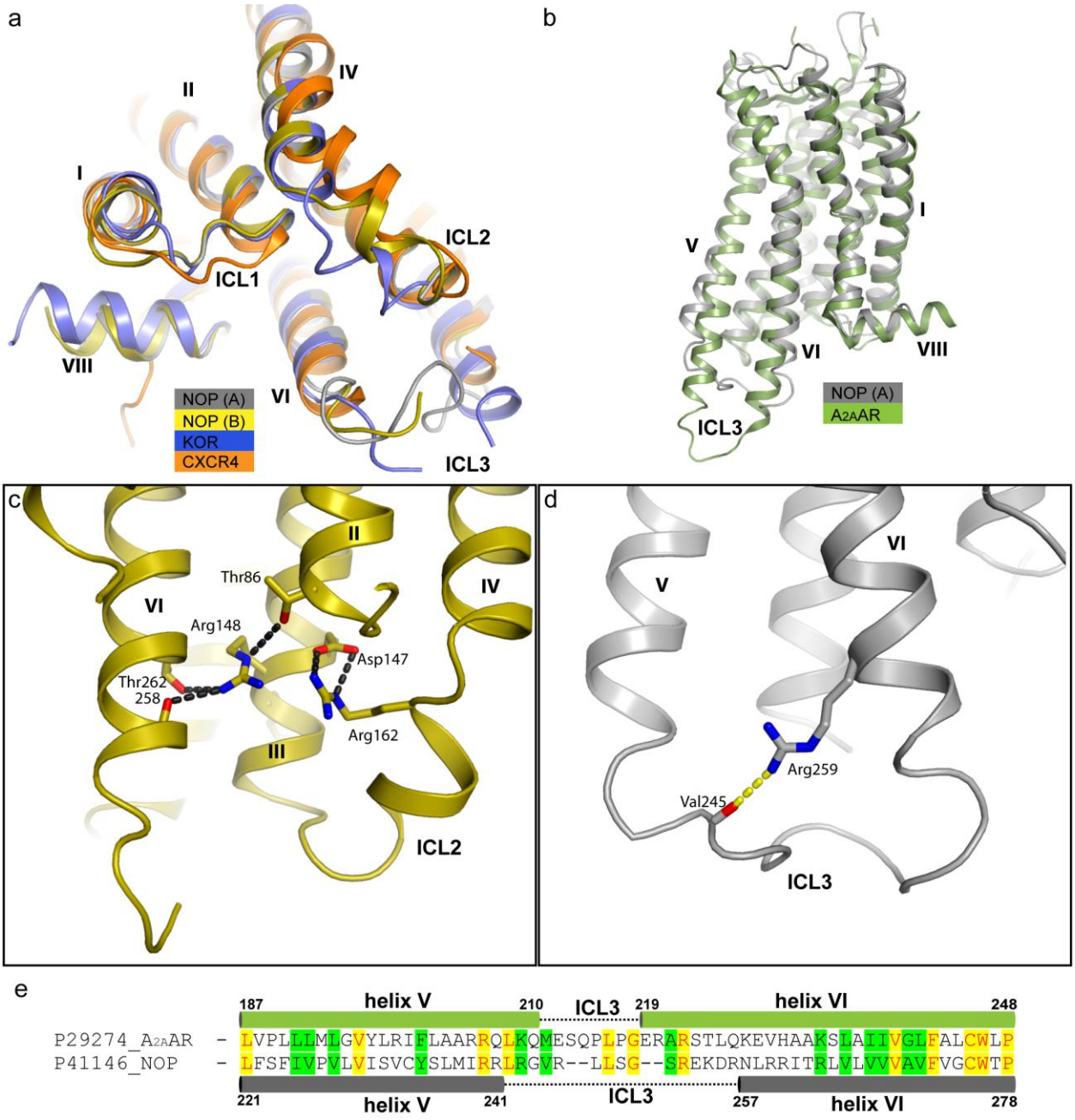

Supplementary Figure 7. The Intracellular Region of NOP. (**a**) Structural superposition of the NOP receptor molecule 'A' and 'B', κ-OR[5] (PDB ID 4DJH), and CXCR4[6] (PDB ID 3ODU) colored gray, yellow, blue, and orange, respectively. (**b**) Structural superposition of the NOP receptor molecule 'B' and thermostabilized $A_{2A}AR$[7] (PDB ID 3PWH) highlighting similarities of ICL3. (**c**) Arg162$^{3.64}$ near the center of ICL2 forms two hydrogen bonds with Asp147$^{3.49}$ of the highly conserved helix III D(E)RY motif constraining this loop close to the IC cavity. The

D(E)RY motif is also engaged in several other hydrogen bonding interactions that link helices III, II and VI. (**d**) Arg259$^{6.31}$ forms a hydrogen bond with the backbone carbonyl with Val245^{ICL3} thereby constraining ICL3 to the 7TM core. (**e**) Sequence alignment of A_{2A}AR and NOP (UniProt ID indicated) highlighting differences in ICL3. This comparison shows that helices V and VI of A_{2A}AR are longer (also see panel b), but ICL3 loop region is shorter compared with the NOP structure. The amino acid lettering for identical and chemically conserved residues is colored with yellow and green background, respectively.

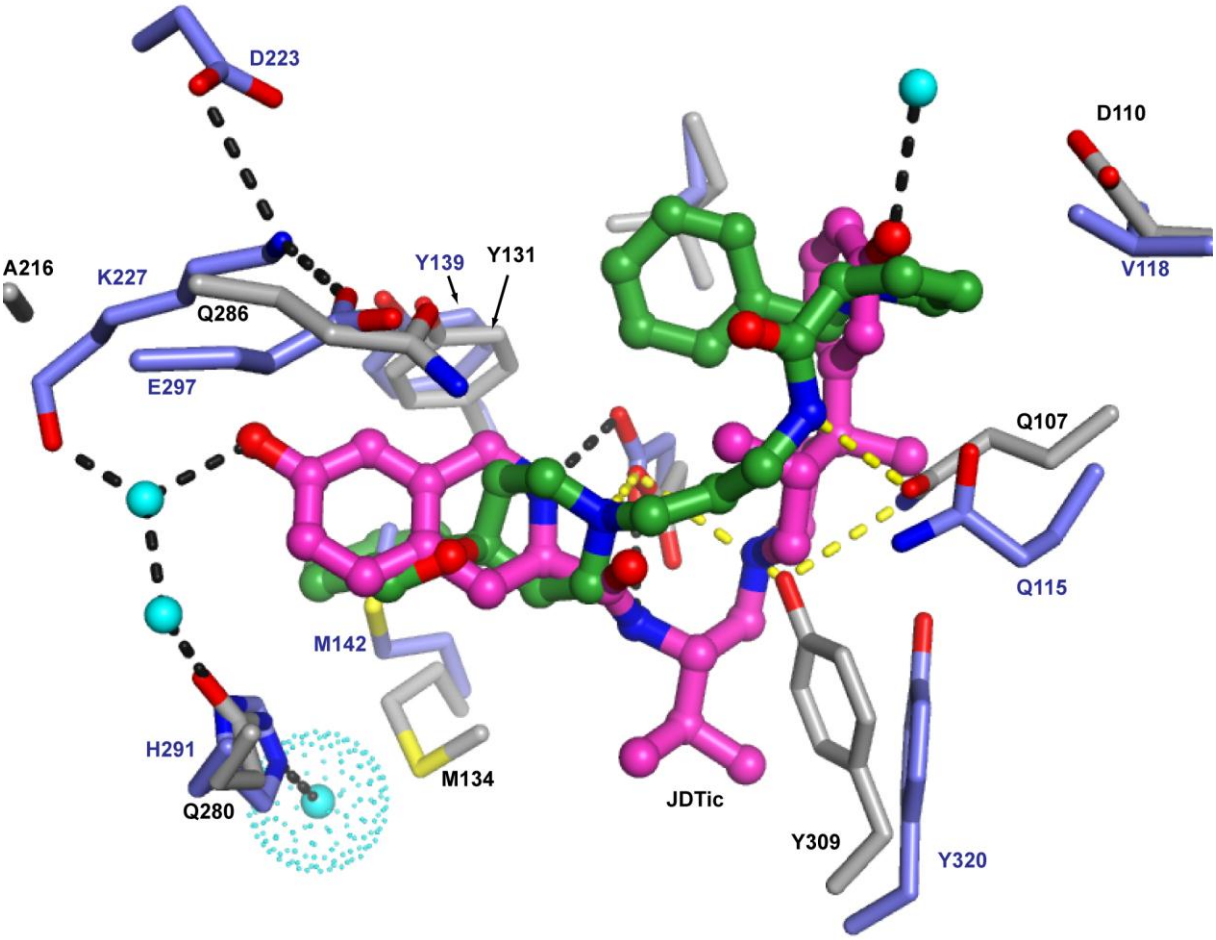

Supplementary Figure 8. Superposition of the NOP and κ-OR highlighting the residues of the respective binding pockets and their bound ligands. Structural alignment of the NOP/C-24 structure (gray with C-24 colored green) and the κ-OR /JDTic structure[5] (PDB ID 4DJH; blue with JDTic colored magenta and waters colored cyan) The residues that are involved in specific interactions with the ligands are depicted as sticks, and the hydrogen bonds are colored yellow and black for the NOP receptor and κ-OR, respectively.

Literature Cited

1 Chen, V. B. *et al.* MolProbity: all-atom structure validation for macromolecular crystallography. *Acta Crystallogr D* 66, 12-21, (2010).

2 Kimple, A. J. *et al.* Structural determinants of G-protein alpha subunit selectivity by regulator of G-protein signaling 2 (RGS2). *J Biol Chem* 284, 19402-19411, (2009).

3 Alexandrov, A. I., Mileni, M., Chien, E. Y., Hanson, M. A. & Stevens, R. C. Microscale fluorescent thermal stability assay for membrane proteins. *Structure* 16, 351-359, (2008).

4 Thompson, A. A. *et al.* GPCR stabilization using the bicelle-like architecture of mixed sterol-detergent micelles. *Methods* 55, 310-317, (2011).

5 Wu, H. *et al.* Structure of the human kappa opioid receptor in complex with JDTic. *Nature* XX, XX-XX, (2012). [Epub online 21 Mar 2012]

6 Wu, B. *et al.* Structures of the CXCR4 chemokine GPCR with small-molecule and cyclic peptide antagonists. *Science* 330, 1066-1071, (2010).

7 Dore, A. S. *et al.* Structure of the adenosine A(2A) receptor in complex with ZM241385 and the xanthines XAC and caffeine. *Structure* 19, 1283-1293, (2011).